~~Resolving~~ Exploring the ocean mesoscale at reduced computational cost with FESOM 2.5: efficient modeling strategies applied to the Southern Ocean ~~: efficient modeling approaches applied to the Southern Ocean~~

Nathan Beech[1], Thomas Rackow[2], Tido Semmler[3], and Thomas Jung[1,4]

1. Alfred Wegener Institute Helmholtz Center for Polar and Marine Research, Bremerhaven, Germany

2. European Center for Medium-range Weather Forecasts, Bonn, Germany

3. Met Eireann, the Irish Meteorological Service, Dublin, Ireland

4. Department of Physics and Electrical Engineering, University of Bremen, Bremen, Germany

Corresponding Author: Nathan Beech (Nathan.beech@awi.de)

12   **Abstract**

13   Efficiency-maximizing modeling strategies are applied to 3 km simulations of the Southern

14   Ocean in past, present, and future climates. The model setup exploits reduced-resolution spin-up and

15   transient simulations to initialize a regionally refined, high-resolution ocean model during short time

16   periods. ~~Several cost-efficient, high-resolution modeling approaches are applied to simulations of the~~

17   ~~Southern Ocean in past, present, and future climates.~~ The results are compared with satellite altimetry

18   data and more traditional eddy-present simulations and evaluated based on their ability to reproduce

19   observed mesoscale activity and to reveal a response to climate change distinct from natural

20   variability~~compared with observations and an ensemble of medium-resolution, eddy-present simulations~~

21   ~~and evaluated based on their ability to reproduce observed mesoscale activity and to reveal a response to~~

22   ~~climate change distinct from natural variability~~. The high-resolution simulations reproduce the observed

23   magnitude of Southern Ocean eddy kinetic energy (EKE) well, but differences remain in local magnitudes

24   and the ~~spatial~~ distribution of EKE. The coarser, eddy-p~~resent~~ermitting ensemble simulates a similar

25   pattern of EKE, but underrepresents observed levels by 5~~0~~5%. ~~Five years of simulated data in each time~~

26   ~~period is found to produce consistent results when evaluating mean conditions and assessing change in~~

27   ~~the region as a whole.~~ At approximately 1 °C of warming, the high-resolution simulations produce no

28   change in overall EKE, in contrast to full ensemble agreement regarding ~~to the increase projected~~EKE

29   rise within~~by~~ the eddy-permitting simulations~~ensemble and despite full ensemble agreement~~. At

30   approximately 4 °C of warming, both datasets produce consistent levels of EKE rise in relative terms,

31   although not absolute magnitudes, as well as an increase in EKE variability. Simulated EKE rise is

32   concentrated where flow interacts with ~~topographic~~ bathymetric features in regions already known to be

33   eddy-rich. Regional EKE change in the high-resolution simulations is consistent with changes seen in at

34   least four of five eddy-permitting ensemble members at 1 °C of warming, and all ensemble members at 4

35   °C. However, substantial noise would make these changes difficult to distinguish from natural variability

36   without an ensemble.

Plain Language Summary

Ocean models struggle to simulate small-scale ocean flows due to the computational cost of high-resolution simulations. Several cCost-reducing modeling strategies strategies are applied to high-resolution simulations of the Southern Ocean in a changing climate. andThey are evaluated with respect to observations and traditional, lower-resolution modelling methods. The high-resolution simulations effectively reproduce small-scale ocean flows seen in satellite data and are largely consistent with traditional model simulations regarding their response to climate changeafter 4 °C of warming. Small-scale flows are found to intensify near bathymetric features and to become more variable.

1 Introduction

Mesoscale activity in the Southern Ocean has been the subject of much research and interest in recent years due to the intensification of Southern Hemisphere westerlies (Marshall, 2003), the phenomena of eddy saturation and compensation (Munday et al., 2013; Bishop et al., 2016), and the potential for carbon sequestration in the face of ongoing anthropogenic emissions (Sallée et al., 2012; Landschützer et al., 2015; Frölicher et al., 2015). Satellite oObservations already reveal an intensification of eddy activity in the Antarctic Circumpolar Current (ACC) and changes are attributed primarily to wind stress (Marshall, 2003; Hogg et al., 2015; Martínez-Moreno et al., 2021). Modeling studies have been able to reproduce the observed changes, as well as project continued intensification throughout the 21st century (Beech et al., 2022), but the modeled results rely on only partially resolved eddy activity relative to observations, leaving open the possibility for new findings or greater clarity.

Advances in computational capabilities have enabled ocean modeling science to make great progress in overcoming the substantial computational burden of simulating the mesoscale., butHowever, shortcomings remain, particularly in the Southern Ocean where the Rossby radius can be as small as 1 km, increasing the computational cost of resolving eddies (Hallberg, 2013). Even model resolutions that can generally be considered eddy-resolving are only eddy-permitting poleward of 50° if grid spacingthey does not vary in space (Hewitt et al., 2020). This highlights an efficiency challenge in simulating the mesoscale with traditional model grids; resolutions necessary to resolve high-latitude, small-radius eddies are both prohibitively expensive and unnecessary to resolve mesoscale eddies in the lower latitudes. Fortunately, a growing number of modelling alternatives to traditional grids now enable dynamic spatial allocation of resources (Danilov, 2013; Ringler et al., 2013; Danilov et al., 2017; Jungclaus et al., 2022), creating the opportunity to more efficiently resolve the mesoscale.

As resource allocation in high-resolution modeling becomes spatially flexible in the pursuit of more efficient configurations, the temporal component must also be scrutinized for efficiency. Traditional modeling approaches require long spin-up periods in order to equilibrate the deep ocean and reduce

71 model drift (Irving et al., 2021). Although the impacts of drift are not negligible, they~~it~~ generally affect~~s~~

72 large-scale processes in the deep ocean; mesoscale processes that require high resolutions to simulate are

73 typically fast-to-equilibrate and will appear relatively quickly wherever large-scale ocean conditions lead

74 to their creation. Admittedly, one cannot entirely disentangle the two scales, as mesoscale activity does

75 affect the position of fronts, stratification, and the paths of ocean circulation (Marshall et al., 2002;

76 Marzocchi et al., 2015; Chassignet and Xu, 2017). Yet, with equilibration times for the deep ocean on the

77 scale of thousands of years (Irving et al., 2021), the possibility, and ultimately necessity, to reduce the

78 resolution of spin-up runs relative to production runs must be investigated.

79 Advancing the concept of dynamic temporal allocation of resources further, the traditional

80 transient climate change simulation also represents an efficiency bottleneck for some applications; by

81 modifying the climate continuously in time, each year of a transient simulation is effectively a single

82 realization of a global mean climatic state that varies from the following and preceding years by only a

83 fraction of a degree. For some applications, like hindcasts of real events or trend analysis, this approach

84 may be desirable, but for assessing the impacts of climate change with limited resources and a low signal-

85 to-noise ratio, a larger sample of realizations for a consistent climatic state may be more suitable.

86 Aside from oceanic concerns, the atmosphere can have substantial impacts on mesoscale activity

87 in climate models. Most simply, with a coupled atmosphere, absolute surface winds will react to ocean

88 eddy activity, whereas atmospheric forcing will not, resulting in more eddy killing by wind stress

89 (Renault et al., 2016). Additionally, an atmosphere coupled to a high-resolution ocean must be of

90 similarly high resolution for certain mesoscale interactions to be resolved (Byrne et al., 2016). Ultimately,

91 the modeled atmosphere further escalates the already exponential cost of increasing ocean resolution by

92 requiring more computational resources in order for the benefits of the resolved mesoscale to fully

93 transfer to the broader climate.

94 To address the computational inefficiencies outlined above, a~~n experimental~~ novel simulation

95 configuration is proposed, combining several experimental modeling approaches. Simulations will exploit

96   the multi-resolution Finite volumE Sea-ice Ocean Model (FESOM) (Danilov et al., 2017) employing a

97   high-resolution unstructured mesh that concentrates computational resources on the Southern Ocean,

98   while maintaining grid resolution in the remainder of the global ocean that can still be considered high-

99   resolution, as in, for example, HighResMIP (Haarsma et al., 2016). The multi-resolution strategy

100   overcomes the efficiency challenges of resolving high-latitude eddies without needlessly increasing

101   tropical resolutions, as well as limiting the focus and computational requirements to one hemisphere. The

102   high-resolution simulations will make use of a spin-up simulation on a medium-resolution, eddy-

103   permitting mesh to avoid the computational burden of allowing an eddy-resolving ocean to equilibrate

104   deep, slow-changing processes. The eddy-permitting mesh will also be used to simulate the transient

105   periods between shorter, high-resolution time slices, increasing the signal-to-noise ratio of the results by

106   separating the production data further in time and the progression of anthropogenic climate change.

107   Finally, the ocean model will be forced with atmospheric data from existing coupled simulations

108   (Semmler et al., 2020). Although this will not facilitate mesoscale atmosphere-ocean interaction, the

109   simulation will reflect the climatic development of an eddy-permitting simulation of the future

110   atmosphere without the additional computational requirements.

111   The Southern Ocean is one of the world's hotspots for mesoscale activity and a region where

112   substantial change is anticipated in the context of anthropogenic climate change (Beech et al., 2022).

113   Simultaneously, the high latitude of the region makes eddy-resolving model simulations computationally

114   demanding and observational data relatively scarce (Auger et al., 2023; Hallberg, 2013). Yet, as the

115   climate changes, the importance of the Southern Ocean grows as a heat and carbon sink, an ecosystem,

116   and a medium for feedback between the atmosphere and ocean (Byrne et al., 2016; Frölicher et al., 2015).

117   Thus, the study of the Southern Ocean demands innovation in the modeling field to produce high-

118   resolution simulations at reduced computational cost. This study maximizes grid resolution relative to

119   computational cost using an unstructured, multi-resolution grid, a medium-resolution spin-up simulation,

120   and atmospheric forcing from lower-resolution coupled simulations in order to focus resources as much as

121 possible on resolving mesoscale activity in the study region. The resulting simulations enable an

122 exploratory analysis of the past, present, and future of the Southern Ocean with a fully resolved

123 mesoscale. Simulations with this cost-efficient, high-resolution configuration are presented in comparison

124 to a comprehensive ensemble of eddy-permitting simulations to assess the performance of the efficiency-

125 focused approach in reproducing mesoscale activity and its response to climate change.

126 **2   Methods**

127 **2.1 Experimental setup**

128

129   This analysis contrasts is broadly a comparison of results from a subset of simulations from AWI-

130 CM-1-1-MR's contribution to the sixth phase of the Coupled Model Intercomparison Project (CMIP6;

131 (Semmler et al., 2020). AWI-CM-1-1-MR's contribution to CMIP6 (hereafter referred to as the AWI-

132 CM-1 ensemble) (Semmler et al., 2020) withand single-member stand-alone ocean simulations using an

133 updated version of FESOM (FESOM 2.5) and a mesh substantially refined to a resolution reaching less

134 thansurpassing 3 km in the Southern Ocean (hereafter referred to as the SO3 simulations) (Supplementary

135 Figure 1). Observations of ocean surface velocity derived from satellite altimetry data are also used to

136 evaluate the model performance of each simulationmodel performance for both modeled datasets during

137 the period of overlap with the altimetry record. The AWI-CM-1 simulations consist of the five-member

138 ensemble of historical simulations and the five-member ensemble of climate change projections under

139 shared socioeconomic pathway (SSP) 3-7.0 which were performed by AWI-CM-1-1-MR in CMIP6

140 (Semmler et al., 2020). These areare state-of-the-art CMIP6 experiments and benefit from the multiple

141 ensemble members and long spin-up times that CMIP simulations typically boast. However, while the

142 AWI-CM-1 ensemble reproduces eddy activity remarkably well within the context of CMIP6 (Beech et

143 al., 2022), high-resolution ocean modeling now far surpasses even the highest ocean resolutions in the

144 CMIP6 ensemble. Conversely, the SO3 simulations push the limits of ocean resolution but rely on several

145 measures for maximizing computational efficiency that may impact the robustness of the simulations.

146 Details on the experimental setup for CMIP6 and ScenarioMIP are widely available (Eyring et al., 2016;

147 O'Neill et al., 2016) and information more specific to AWI-CM-1-1-MR's contribution has been

148 published previously (Semmler et al., 2020). The following sections will outline the details of the SO3

149 simulations.

150 To produce initial conditions for the high-resolution model simulations on the SO3 mesh,~~The~~

151 ~~model experiments with SO3 consist of~~ a medium-resolution, eddy-permitting, ocean-only transient

152 simulation was first run from 1851 to ~~-~~2100 using the same ocean mesh employed by AWI-CM-1-1-MR

153 in CMIP6 (Semmler et al., 2020). This mesh has~~and three shorter simulations with the SO3 mesh at~~

154 ~~different time periods during the progression of anthropogenic climate change. The medium-resolution~~

155 ~~transient run is a stand-alone ocean simulation using a medium-resolution mesh that has~~ been shown to

156 effectively reproduce eddy activity in active regions while maintaining a computational cost comparable

157 to a traditional ¼ ° model (Beech et al., 2022). The transient simulation~~model~~ wa~~i~~s initialized with

158 conditions for ocean temperature and salinity, as well as sea ice concentration, thickness, and snow cover

159 taken from the end of the first year (1850) and first ensemble member (r1i1p1f1) of AWI-CM-1-1-MR's

160 historical simulations in CMIP6 (Semmler et al., 2018, 2020, 2022a, b). In this way, the model undergoes

161 a semi-cold start in which ocean conditions are not exact continuations of the previous coupled

162 simulation, but should be far closer to equilibrium than a true cold start initialization~~nonetheless benefit~~

163 ~~from more realistic and partially equilibrated ocean properties. The~~stand-alone ocean is eddy-permitting

164 transient simulation was forced using atmospheric data from the same ensemble member of the historical

165 CMIP6 simulations until 2014 (Semmler et al., 2022a), and thereafter using the first ensemble member of

166 AWI-CM-1-1-MR's ScenarioMIP simulations for ~~shared socioeconomic pathway (~~SSP~~)~~ 3-7.0 (Eyring et

167 al., 2016; O'Neill et al., 2017; Semmler et al., 2022b). This approach to forcing takes advantage of a

168 coupled simulation, CMIP6, to produce a forcing dataset of better temporal and spatial coverage than the

169 observational record and which maintains a realistic transient climate throughout anthropogenic impacts

170 during the 21st century.

171   In the years 1950, 2015, and 2090, the modelFESOM is reinitialized with the higher-resolution

172 ocean grid, SO3 (Supplementary Figure 1), using the same semi-cold start approach and forcing dataset

173 that was implemented for the eddy-permitting transient simulation described previously. These years were

174 chosen to represent a historical period, beginning in 1950, when the effects of climate change on EKE

175 should be small or none (Beech et al., 2022); a near-present period, beginning in 2015, in which the

176 simulations will overlap with satellite altimetry data; and a projected period, beginning in 2090, which

177 should include a strong climate change signal. The latter two simulated periods represent 1.07 °C and

178 3.74 °C of warming, respectively, in the first ensemble member of the AWI-CM-1 ensemble defined as a

179 rise in the 21-year running mean of global mean two-meter air temperatures. Warming of the ensemble

180 mean is similar: 1.08 and 3.76 °C respectively, and warming is henceforth approximated as 1 °C and 4 °C

181 in Figure 4 and the text. as well as Iinitial conditions for these shorter time-slice simulations are taken

182 from the end of the previous year of the eddy-permittingeddy-permitting transient simulation. The high-

183 resolution simulations are each integrated for six years with the first year ignored as a true spin-up,

184 leaving five years of data for each time period. While model drift may be a concern with such a short true

185 spin-up period, this should affect each of the high-resolution time slices similarly and to a limited extent

186 due to their short integration lengths. Thus, the differences between the high-resolution ocean simulations

187 should primarily reflect anthropogenic climate impacts simulated during the eddy-permitting transient

188 run. The high-resolution grid is, in truth, a regionally refined mesh in which a 25 km global resolution is

189 increased refined to approximately 2.5 km, following (Danilov, (2022), primarily south of 40 °S, but with

190 other pertinent regions, such as the Agulhas Current and several narrow straits, also refined. In this way,

191 the model is able to simultaneously achieve eddy-rich conditions in the Southern Ocean and many of the

192 nearby active regions, as well as a global resolution that would still be considered high in the context of

193 CMIP6 (Hallberg, 2013; Hewitt et al., 2020). While model drift may be a concern with such a short true

194 spin-up period, this should affect each of the high-resolution time slices similarly and to a limited extent

195 due to their short integration lengths. Thus, the differences between the high-resolution ocean simulations

196 should primarily reflect anthropogenic climate impacts simulated during the eddy-permitting transient run

197 and present in the forcing dataset. ~~The high-resolution simulations are each integrated for six years with~~

198 ~~the first year ignored as a true spin-up, leaving five years of data for each time period. While model drift~~

199 ~~may be a concern with such a short true spin-up period, this should affect each of the high-resolution time~~

200 ~~slices similarly and to a limited extent due to their short integration lengths. Thus, the differences between~~

201 ~~the high-resolution ocean simulations should primarily reflect anthropogenic climate impacts simulated~~

202 ~~during the eddy-permitting transient run.~~

203 **2.2 Model configuration**

204 The Finite volume Sea-ice Ocean Model version 2.5 is a post-CMIP6 era model, having been

205 refactored to a finite-volume configuration from the finite-element version (FESOM1.4, Q. Wang et al.,

206 2014) employed in CMIP6, and transitioned to arbitrary Lagrangian Eulerian ~~(ALE)~~ vertical coordinates,

207 among other improvements (Danilov et al., 2017; Scholz et al., 2019, 2021). FESOM's most

208 distinguishing feature among mature ocean models is the unstructured horizontal grid that exploits

209 triangular grid cells which can smoothly vary in size to change the horizontal grid resolution in space. In

210 these simulations, full free surface, or z*, vertical coordinates were used, allowing the vertical model

211 layer thicknesses to change in time. Gent-McWilliams eddy parameterization (Gent and McWilliams,

212 1990) is scaled with resolution according to ~~(~~Ferrari et al.~~,~~ (2010) and vertical mixing is simulated by a *k*-

213 profile parameterization scheme (Large et al., 1994).

214 The SO3 mesh consists of over 22 million surface elements (triangle faces) or 11 million surface

215 nodes (triangle vertices) and 70 vertical layers~~.~~. The simulations produce about 1.1 terabytes of data per

216 year of 3D data stored on nodes. For reference, the medium-resolution mesh used in the AWI-CM-1

217 ensemble is 1.6 million surface elements or 0.83 million surface nodes and 46 vertical layers and

218 produces approximately 56 GB per year of 3D data stored on nodes. The model was run on 8192 CPU

219 cores and with a typical throughput of approximately 0.65 simulated years per day, consuming

220 approximately 5.5 million CPU hours in total despite the various cost-saving modeling approaches. It

221 should be noted, however, that the throughput in high-resolution production simulations like this is highly

222 dependent on the volume and choice of data being saved. The simulations and following analysis were

223 performed using the high-performance computing system, Levante, at the German Climate ~~Research~~

224 Computing Center (DKRZ).

225   The ocean model is forced by several atmospheric variables at a six-hour resolution, although one

226 forcing variable, humidity, is interpolated monthly data. The forcing data is ~~first interpolated to a regular~~

227 ~~grid which can be interpreted by the model and applied~~supplied to the model on the regular atmospheric

228 grid used in the coupled setup during AWI-CM-1-1-MR's CMIP6 simulations (Semmler et al., 2018) and

229 interpolated to the multi-resolution grid used in the respective simulations by FESOM. Runoff data is a

230 monthly climatology and dynamic ice sheet coupling is not included, meaning the freshwater influx from

231 the Antarctic continent does not react to warming which may impact certain processes, such as the timing

232 and intensity of sea ice loss (Pauling et al., 2017; Bronselaer et al., 2018).

233 **2.3 ~~Geostrophic~~ Modeled ocean velocity data~~ies~~**

234 ~~   Ocean velocities in the SO3 simulations are saved on a daily timescale as direct model output,~~

235 ~~whereas~~

236 ~~   (Semmler et al., 2018) in the AWI-CM-1 ensemble, only monthly data is available and daily data~~

237 ~~must first be derived from sea surface height data and geostrophic balance as in equations (1) and~~

238 ~~(2).~~Geostrophic balance is an idealized approximation that does not match real ocean velocities for

239 several reasons, including the presence of ageostrophic flow, such as Ekman transport, as well as

240 assumptions made in the derivation of equations (1) and (2). Specifically, geostrophic balance between

241 the Coriolis effect and the pressure gradient is valid under the assumption that the curl of horizontal

242 velocities or vorticity is small relative to the magnitude of overall flow. In models, this assumption is

243 relatively close to reality in coarse-resolution simulations where geostrophic flow dominates, but on

244 higher-resolution meshes, where submesoscale flows are well-resolved, these omitted terms become

245 larger. Therefore, while using geostrophic velocities for both high-resolution and coarse-resolution

246 modeled datasets would be methodologically consistent, the error introduced would be systemically larger

247 for the finer-resolution dataset than the coarser. Therefore, we do not consider the use of geostrophic

248 velocities for both modeled datasets in this analysis to bring the data into closer agreement. Rather, for the

249 AWI-CM-1 dataset, where daily ocean velocities were not saved (Semmler et al., 2018), geostrophic

250 velocities derived from sea surface height with equations (1) and (2) are the best possible choice, and

251 fortunately, as described earlier, the error introduced by the assumptions of geostrophic balance will be

252 small. For the SO3 simulations, direct model output was saved and is preferred, particularly given the

253 high resolution of the mesh. (Taburet et al., 2019)

254 $u = -g/f * \partial SSH/\partial y$ ⠀⠀⠀⠀⠀⠀⠀⠀(1)

255 $v = g/f * \partial SSH/\partial x$ ⠀⠀⠀⠀⠀⠀⠀⠀(2)

256

257 The omission of Ekman transport, the primary source of ageostrophic oceanic flow from atmospheric

258 influences, can be relatively well addressed in the SO3 dataset by selecting modeled velocities just below

259 the Ekman layer. At depths of 25-30m below sea level, the bulk of Ekman transport can be avoided (Price

260 et al., 1987), while velocities should not substantially differ from those at the surface. What ageostrophic

261 flow remains in the model output velocities should be primarily large-scale and overshadowed small

262 relative to by geostrophic flow in the high-energy regions of the ocean, including the ACC (Yu et al.,

263 2021).

264 **2.4 Altimetry data**

265 ⠀⠀⠀An observational data product of gridded, daily geostrophic velocities derived from along-track

266 satellite altimetry from crossover data is taken from the Data Unification and Altimeter Combination

267 System (DUACS) (Taburet et al., 2019). The gridded product has a resolution of 0.25 °, although

268 effective resolution at high latitudes may be much lower (Ballarotta et al., 2019). Recently, improved data

269 has become available in the ice-covered regions of the Southern Ocean (Auger et al., 2022), but does not

270 yet cover the full present-day simulated period (2016-2020) in this study. Absolute velocities from the

271 gridded altimetry product were used to calculate anomalies and EKE using equations (3) and (4) below

272 for consistency with the modeled dataset.

273 ~~To avoid including ageostrophic contributions to ocean surface velocity in this analysis, model output~~

274 ~~velocity between 25 m and 30 m depth is used for the SO3 dataset. This depth should be close enough to~~

275 ~~the surface to closely match surface geostrophic flows while also avoiding Ekman transport, a major~~

276 ~~contributor to ageostrophic ocean flow. What ageostrophic flow remains in the model output velocities~~

277 ~~should be primarily large-scale and overshadowed by geostrophic flow in the high-energy regions of the~~

278 ~~ocean, including the ACC (Yu et al., 2021).~~

279 ~~u = −g/f*∂SSH/∂y~~   ~~(1)~~

280 ~~v = g/f*∂SSH/∂x~~   ~~(2)~~

281 **~~e.~~ 2.5 EKE analysis**

282   Velocity anomalies are defined by subtracting the multi-year monthly climatology of each

283 respective 5-year period from daily velocities with equation (3).

284 $u'_i = u_i - \overline{u_m}$ (3)

285 Where u_i is the daily zonal velocity, $'$ denotes an anomaly, and $\overline{u_m}$ is a monthly mean. For meridional

286 velocities (v) substitute u with v.

287 Eddy kinetic energy is calculated from ocean velocities according to equation (4).

288 $EKE_i = 0.5(u'^2_i + v'^2_i)$ (4)

289   Where ($_i$) denotes a daily value and ($'$$-$) denotes an anomaly.

290   EKE was calculated on the native grid of each dataset and then interpolated to a 0.25 ° grid for all

291   analyses. I EKE in Figures 1 and 3, EKE was first calculated on a daily timescale and coarsened to five-

292   day means before analysis to reduce computational costs during post-processing. Area-integrated EKE

293   (Figure 1, 3) is calculated by summing the area-weighted EKE of each grid cell in the study region

294   defined as the zonal band between 45 °S and 650 °S. with tThe Brazil/Malvinas confluence region

295   between 57 °E and 29 °E and northward of 40 °S is removed to focus the study on a region with

296   consistent physical drivers theorized to be responsible for the changes in eddy activity (Beech et al.,

297   2022) (Beech et al., 2022). As a precaution, Each dataset was linearly detrended before analysis in

298   Figures 1 and 3 to avoid artificially increasing the range of the later distributions due to the accelerating

299   climate change signal. Select statistical properties are reported in Supplementary Tables 1-3 to indicate

300   deviations from normality (D'Agostino and Belanger, 1990; Fisher, 1997) and autocorrelation (Durbin

301   and Watson, 1950). Rather than attempt to manipulate the data to meet certain statistical assumptions,

302   complex statistical tests are avoided and the statistical properties reported can be used to interpret the

303   EKE data in a physical sense. EKE anomalies (Figure 1) were calculated by subtracting the 2016-2020

304   mean of area-integrated EKE from the EKE 5-day mean values data oof each period. Normalized EKE

305   was calculated by further dividing EKE anomaly by the standard deviation of EKE during the 2016-2020

306   period. In Figure 4, ensemble agreement is determined by ordering the ΔEKE values within each grid cell

307   from lowest to highest, plotting the positive values in increasing order from left to right and negative

308   values in decreasing order from left to right.

309   **3   Results**

310   **3.1 Agreement with observations**

311   During the five-year period of overlap with observations, the SO3 simulation is a drastic

312   improvement on the AWI-CM-1 ensemble in reproducing median observed EKE (Figure 1a, c); o); only a

313 slight underrepresentation of EKE remains in the SO3 simulation, although the simulated distribution

314 ~~remains~~ is somewhat distinct from observations~~.~~, ~~whereas~~In comparison, the AWI-CM-1 ensemble, being

315 effectively eddy-permitting in the Southern Ocean, underrepresents observations by approximately~~bout~~

316 5~~0~~0% (Figure 1a, c, note the different y-axis). EKE in SO3 appears more variable than the observations

317 considering ~~as can be inferred from the~~its larger range. (Figure 1c, e) ~~and I~~, and in general, the modeled

318 datasets display greater deviations from a normal distribution than the observations (Figure 1a, b, c;

319 Supplementary Table 2). ~~ts distribution appears less Gaussian than observations or the eddy-permitting~~

320 ~~dataset (Figure 1a, b, c). Taking the AWI-CM-1 ensemble as an example, there is no consistent pattern of~~

321 ~~multimodality or skewness and the ensemble mean more closely approximates the normal distribution~~

322 ~~than the individual members (Figure 3), suggesting that deviations from normality could be primarily due~~

323 ~~to sample size rather than the character of the data.(Beech et al., 2022)~~ Nonetheless, ~~r~~Relative to the

324 AWI-CM-1 model bias and the magnitude of EKE resolved, the ensemble spread within the AWI-CM-1

325 dataset is small (Figure 3), suggesting that a single ensemble member of five years duration is sufficient

326 to assess how well a model captures the ~~overall~~ magnitude of overall Southern Ocean EKE (Figure 1c).

327

328
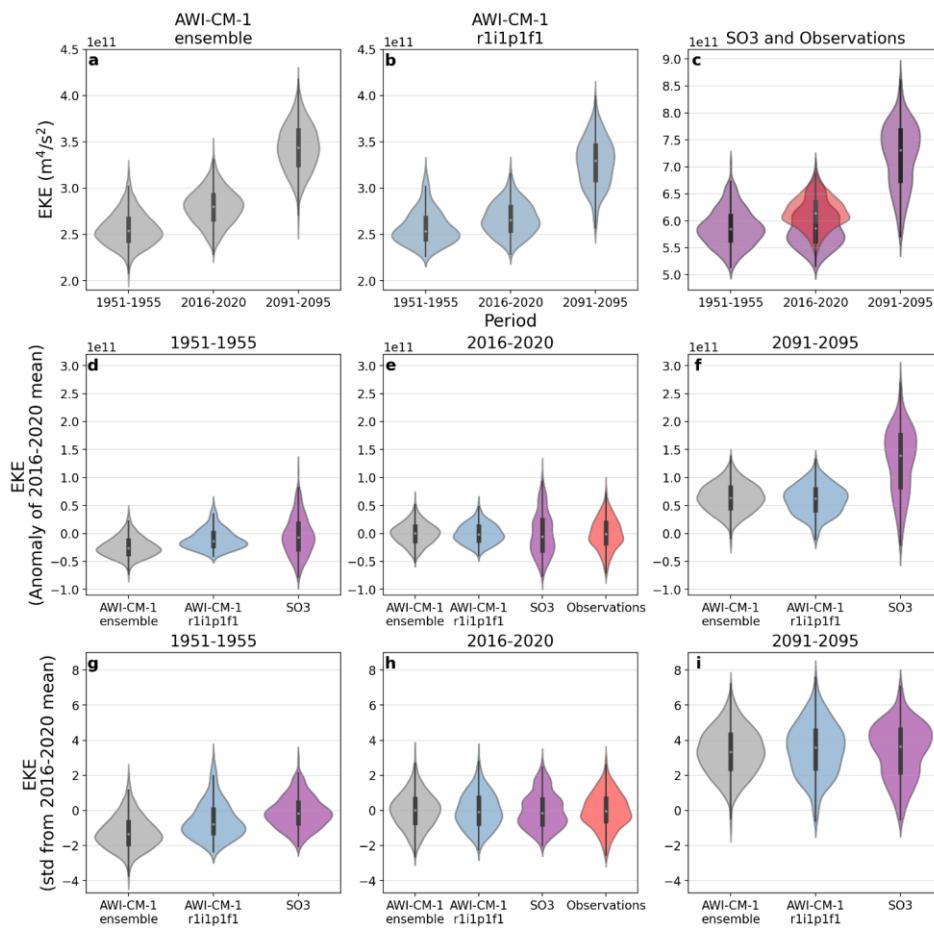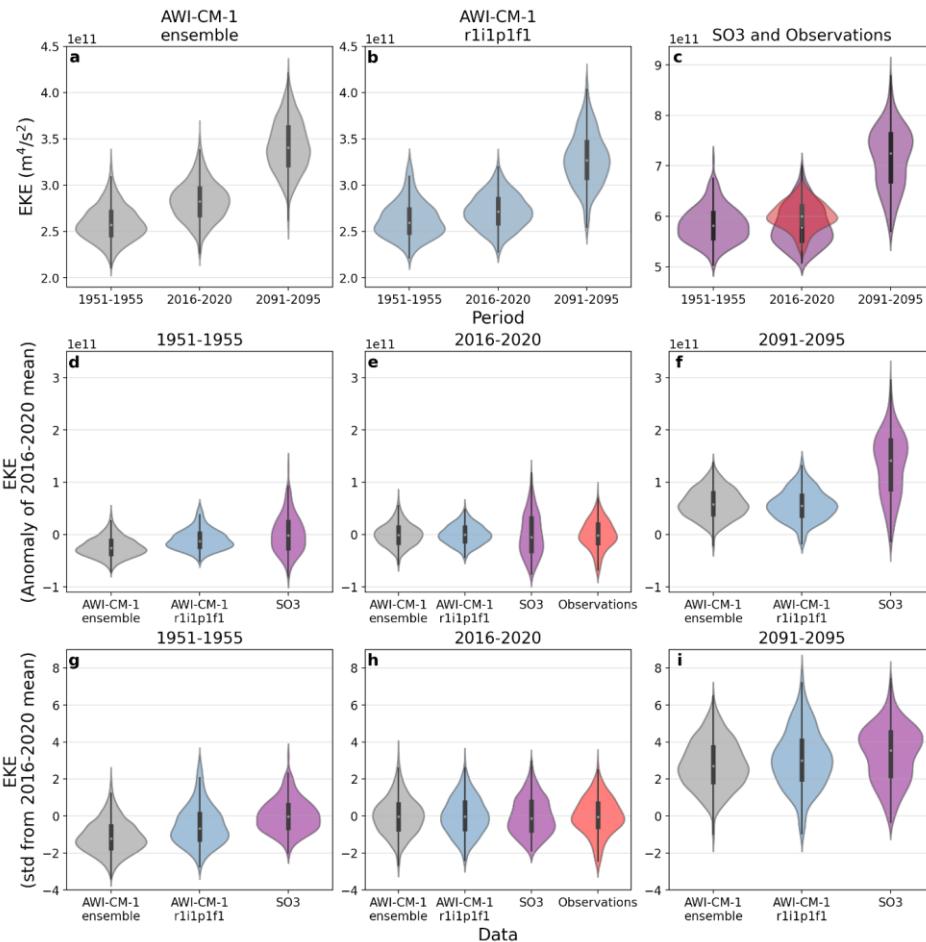
Figure 1. Violin plots of area-integrated Southern Ocean EKE in simulations and observations.

Central points of each plot indicate the median, thick bars span the first and third quartiles, thin bars span

the range, and the violin body is a kernel density estimation of the data. **a-c)** M̶Real ̶magnitudes of area-

integrated EKE (note the different y axes) **a)** The AWI-CM-1 ensemble. **b)** the first member of the AWI-

CM-1 ensemble, from which the SO3 simulations take their atmospheric forcing. **c)** The SO̶o̶3

simulations and observations. **d-f)** A̶E̶K̶E ̶anomalies relative to the 2016-2020 mean of area-integrated

335 EKE for each dataset respectively. **d)** 1951-1955. **e)** 2016-2020. **f)** 2091-2095. **g-i)** Normalized values

336 relative to the mean and standard deviation of EKE during the 2016-2020 period for each dataset

337 respectively. **g)** 1951-1955. **h)** 2016-2020. **i)** 2091-2095.

338   From a regional perspective, the SO3 simulation accurately reflects local magnitudes of observed

339 EKE and also generally captures the spatial distribution well (Figure 2). However, there are regional

340 shortcomings, such as between 90 and 145 °E. Grid resolution in this region should be sufficient to

341 resolve eddy activity (Supplementary Figure 1), indicating that the bias arises from another source. In the

342 AWI-CM-1 ensemble, the regional representation of EKE reinforces a broad underrepresentation relative

343 to observed magnitudes, but the major geographic features of eddy activity are fairly well represented

344 (Figure 2). Once again, the ensemble spread within the AWI-CM-1 simulations reveals remarkable

345 consistency, this time in terms of the spatial pattern and regional magnitudes (Supplementary Figure 2),

346 reinforcing the conclusion that a single ensemble member of five years duration is sufficient to assess the

347 mean state of EKE in the Southern Ocean. The consistency of the AWI-CM-1 ensemble further suggests

348 that regional shortcomings in eddy activity in the SO3 simulations are not a product of variability within a

349 single realization of Southern Ocean conditions (Supplementary Figure 2).

350
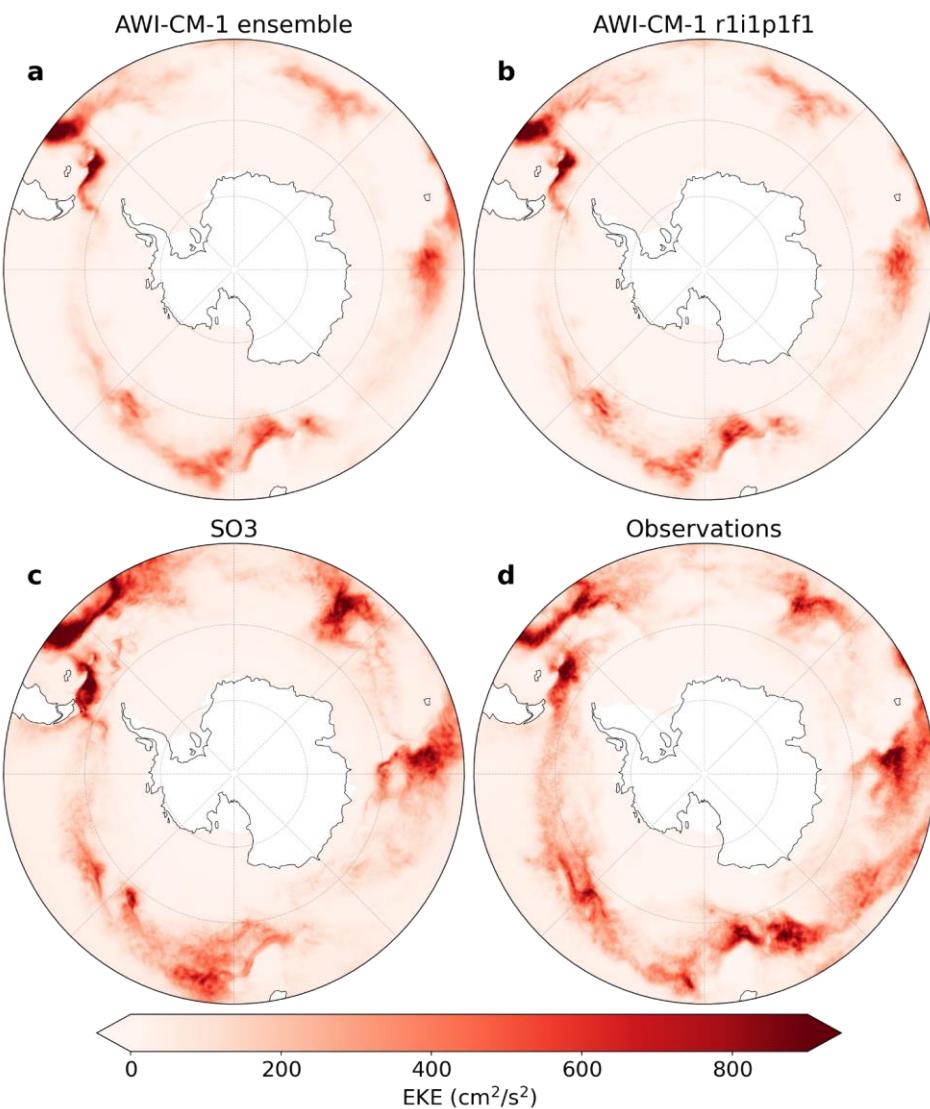
Figure 2. Mean eddy kinetic energy between 2016 and 2020. a) The AWI-CM-1 ensemble. **b)** The first

member of the AWI-CM-1 ensemble. **c)** The SO3 simulation. **d)** The gridded satellite altimetry dataset.

353

3.2 EKE change and significance

Southern Ocean eddy activity has been shown to intensify over the recent decades both using satellite altimetry (Martínez-Moreno et al., 2021), and the complete AWI-CM-1-1 dataset from CMIP6 (Beech et al., 2022). Even after reducing the AWI-CM-1 CMIP6 dataset to five-year periods preceding the apparent change (1951-1955) and at the end of the altimetry era (2016-2020), this intensification is still discernable within the AWI-CM-1 ensemble (Figure 1a). Despite this, the SO3 simulations do not demonstrate any substantial change in EKE magnitude over the same period (Figure 1). Further reducing the ensemble to its individual members (Figure 3), the EKE rise is still relatively ~~relatively clear~~robust in each case, including clear separation of the datasets considering the median, mode, and ~~first and third quartiles~~distribution of the ~~data~~distributions (Figure 3). However, the first ensemble member, from which the atmospheric forcing of SO3 is taken, demonstrates less EKE rise than the ensemble average (Figure 3), suggesting that natural variability in atmospheric conditions may contribute to the disagreement. Further investigation reveals several differences between the SO3 simulations and the AWI-CM-1 ensemble members that may play a role. Mean zonal ocean velocity in SO3 is faster and broader than the AWI-CM-1 ensemble (Supplementary Figure 3), meaning wind speed intensification may be misaligned with peak ocean velocities in SO3, particularly around 47 to 51 °S. Moreover, considerably less zonal wind stress is imparted to the ocean in SO3 despite identical wind speeds as the first AWI-CM-1 ensemble member (Supplementary Figure 4), possibly due to the higher ocean surface velocity.

~~suggesting again, that natural or internal variability is not responsible for the discrepancies between simulations. Therefore, despite the first AWI-CM-1 ensemble member, from which the SO3 simulations receive their atmospheric forcing, producing lower-than-average EKE rise over this period (Figure 3), it is likely that other factors(Renault et al., 2016) also contribute to the lack of change in the SO3 simulations.(Renault et al., 2016)~~

378   The intensification of EKE becomes clear in both the AWI-CM-1 ensemble (Figure 1a), its

379   members (Figure 3), and the SO3 simulations (Figure 1c) by the end of the 21st century. Over this period,

380   the variability of EKE, indicated by the range of the distribution, also increases for each dataset (Figure

381   1f, i). EKE rise in SO3 is approximately ~~three times~~twice that of the AWI-CM1 ensemble in absolute

382   terms (Figure 1f), but expressing EKE as a relative value normalized by the mean and standard deviation

383   of each dataset during the observational period (Figure 1g, h, i), reveals greater consistency between the

384   changes until the end of the 21st century. EKE in each dataset appears to increase by approximately 3.5~~3~~

385   standard deviations, and the range of EKE distributions increases by approximately two~~one~~ to three~~wo~~

386   standard deviations (Figure 1h, i). However, the datasets also tend to become more autocorrelated, which

387   can inflate the distribution range (Supplementary Tables 1, 3).

388
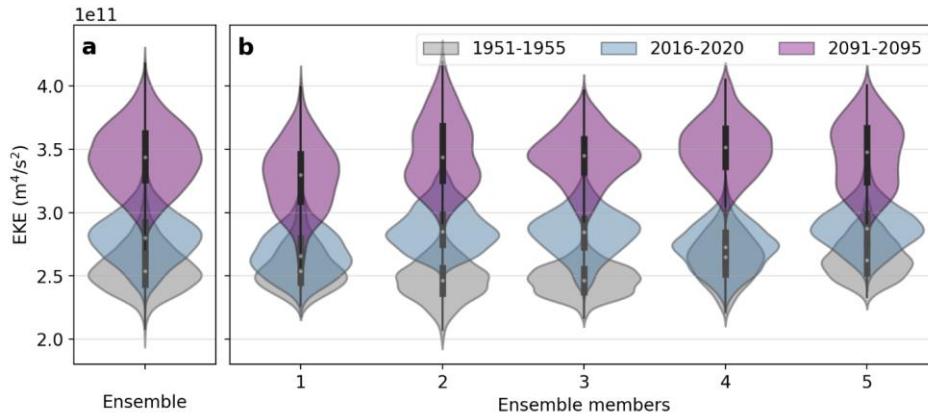
Figure 3. Ensemble spread of EKE in AWI-CM-1. a) Violin plots of area-integratedmean Southern

Ocean EKE in the AWI-CM-1 ensemble. **b)** Violin plots of mean Southern Ocean EKE in each member

of the AWI-CM-1 ensemble. Grey plots represent the period 1951-1955, blue plots represent 2016-2020,

and purple plots represent 2091-2095.

Before considering the regional impacts of warming on EKE in the SO3 simulations, it is useful

to refer to the ensemble spread within the AWI-CM-1 simulations to approximate the reliability of a

single ensemble member in revealing the ensemble-mean change as an analogue to the signal-to-noise

398 ratio. At 1 °C of warming, EKE change in the ensemble is weak, with at least one ensemble member

399 tending to show little or no EKE change in most regions (Figure 4a,c). Only a few clear patterns of

400 change emerge throughout the ensemble, namely the regions of EKE intensification downstream of the

401 Kerguelen Plateau and the Campbell Plateau where four to five out of five ensemble members show clear

402 EKE intensification (Figure 4a). It should be noted that even in these regions of relatively high confidence

403 (4 to 5 ensemble members, Figure 4a) EKE rise can be interspersed with lower-confidence (1 to 2

404 ensemble members, Figure 4c) EKE decline; this is also illustrated by the ensemble mean changes

405 themselves (Supplementary Figures 5̲2, 6̲3). Despite this, the consistency of EKE rise in these regions,

406 and their geographic positions in already EKE-rich regions, suggests that the intensification patterns are

407 robust changes within substantial noise. This level of noise suggests that EKE changes in the SO3

408 simulations at 1 °C of warming will be difficult to distinguish from natural variability when taken on their

409 own; indeed, in the SO3 simulations, the large variability of both sign and magnitude of change within

410 relatively small spatial scales does not lend confidence to any significant change at 1 °C of warming

411 (Figure 5c). However, building on the changes observed in the AWI-CM-1 ensemble, the intensification

412 of EKE downstream of the Kerguelen and Campbell Plateaus seems to be reinforced by the high-

413 resolution simulations.

414
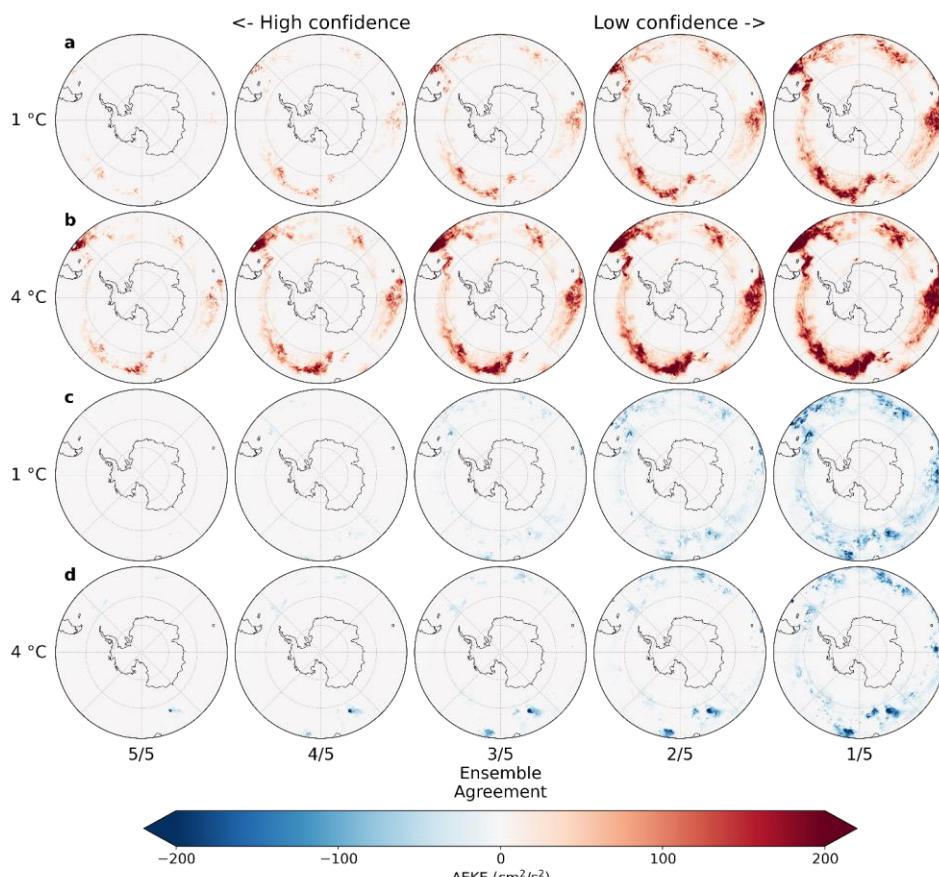
Figure 4. Ensemble agreement regarding EKE change. EKE rise (a, b) and decline (c, d) within the

AWI-CM-1 ensemble after one (a, c) and four (b, d) °C of warming or between 1951-1955 and 2016-

2020 and 2091-2095, respectively, arranged in order of decreasing ensemble agreement regarding change

in each grid cell. Ensemble agreement refers to the number of ensemble members that simulate at least the

pictured magnitude of mean EKE rise or decline for each grid cell. Mean EKE change is defined as the

difference of mean EKE between 1951-1955 and each of the two latter periods, as in Supplementary

Figures 5 and 6 but arranged in ascending order of magnitude for each grid cell and for positive and

negative signs separately. Rank 5/5 indicates the lowest magnitude of mean EKE rise (a, b) or decline (c,

423   d) within the ensemble for a given grid cell, meaning the entire ensemble agrees on at least this much

424   change. Rank 1/5 indicates the highest magnitude of EKE rise or decline within the ensemble for each

425   grid cell, representing the upper limit of projected EKE change.

426

427   At 4 °C of warming, change in eddy activity becomes clearer; EKE intensification downstream of

428   the Kerguelen and Campbell Plateaus is now consistent throughout the entire AWI-CM-1 ensemble, along

429   with additional intensifications south of the Falkland/Malvinas Plateau, around the Conrad Rise, and

430   along the Antarctic Slope Current at approximately 5 °E (Figure 4b). Four fifths of the ensemble also

431   include a broad increase in EKE throughout the ACC across most longitudes. Interestingly, a consistent

432   pattern of EKE decline also emerges upstream of the Campbell Plateau in the entire ensemble (Figure 4d).

433   The spatial pattern of EKE rise is relatively consistent regardless of confidence, with only the magnitude

434   increasing in the lower confidence composites (Figure 4b). The same tendency is observable between the

435   EKE changes at 1 and 4 °C of warming, where the magnitude of change is greater after further warming

436   but follows the same spatial pattern. Thus, regions of intensification can be identified more reliably than

437   the magnitude of change and tend to be concentrated where flow interacts with topographic features, in

438   already eddy-rich regions (Figure 2). Conversely, low confidence EKE decline appears nearly throughout

439   the Southern Ocean in at least one ensemble member, but only consistently upstream of the Campbell

440   Plateau and, to a far lesser extent, downstream of the Drake Passage and Campbell Plateau (Figure 4d).

441   Changes of negative sign tend to be of lower magnitude at 4 °C of warming than at 1 °C. This suggests

442   that ~~in any given single ensemble simulation, a robust general intensification of EKE tends to occur~~the

443   general EKE response to climate change in the Southern Ocean is that of intensification, and the

444   interspersed signals of decline tend to be the result of ~~but can be interspersed with spurious signals of~~

445   ~~decline~~natural variability. Yet, small regions of high-confidence EKE decline ~~are also possible,~~also

446   appear ~~however uncommon~~. Consequently, it would be difficult to confidently separate reliable EKE

447   change from natural variability in simulations without an ensemble to compare with. In the SO3

448 simulations, EKE rise downstream of the Drake Passage and Kerguelen and Campbell Plateaus is

449 substantial (Figure 5f). EKE rise is also projected south of the Falkland/Malvinas Plateau, around the

450 Conrad Rise, and along the Antarctic Slope Current at approximately 5 °E, and a slight EKE decline

451 appears upstream of the Campbell Plateau. All of this is comparable to the AWI-CM-1 ensemble, and the

452 interspersed areas of EKE decline within these regions, for example, around the Conrad Rise, are not

453 improbable based on the example set by AWI-CM-1 (Figure 4d). However, considering that some high-

454 confidence EKE decline is present in the AWI-CM-1 ensemble, it is difficult to confidently dismiss

455 regional EKE decline in the SO3 simulations as noise.

456

457

458
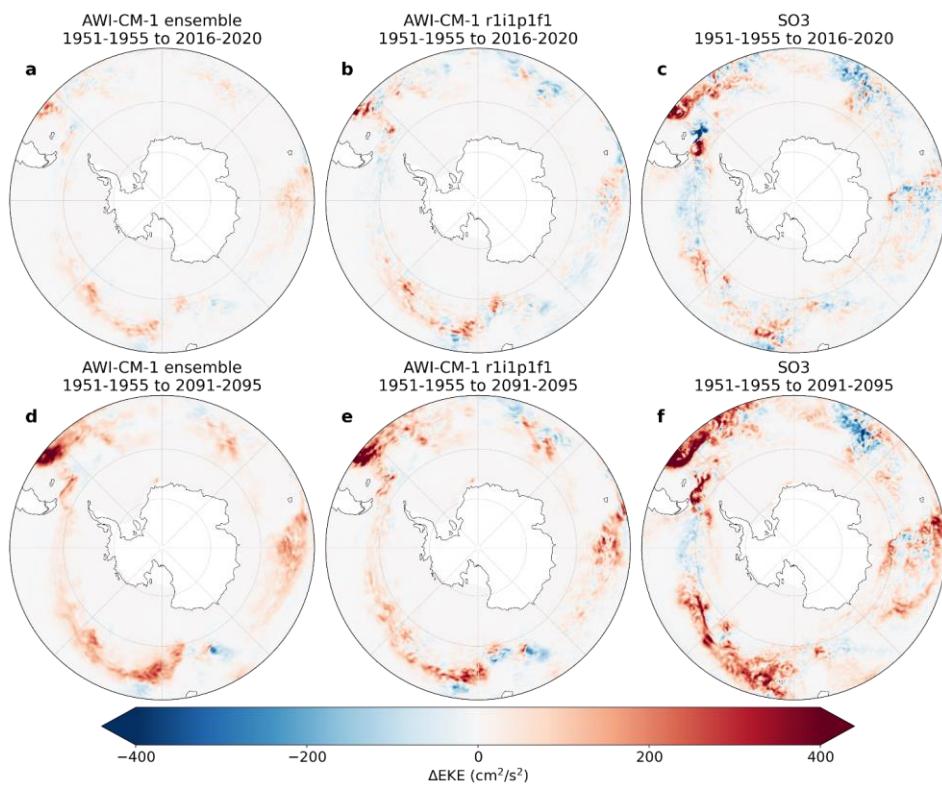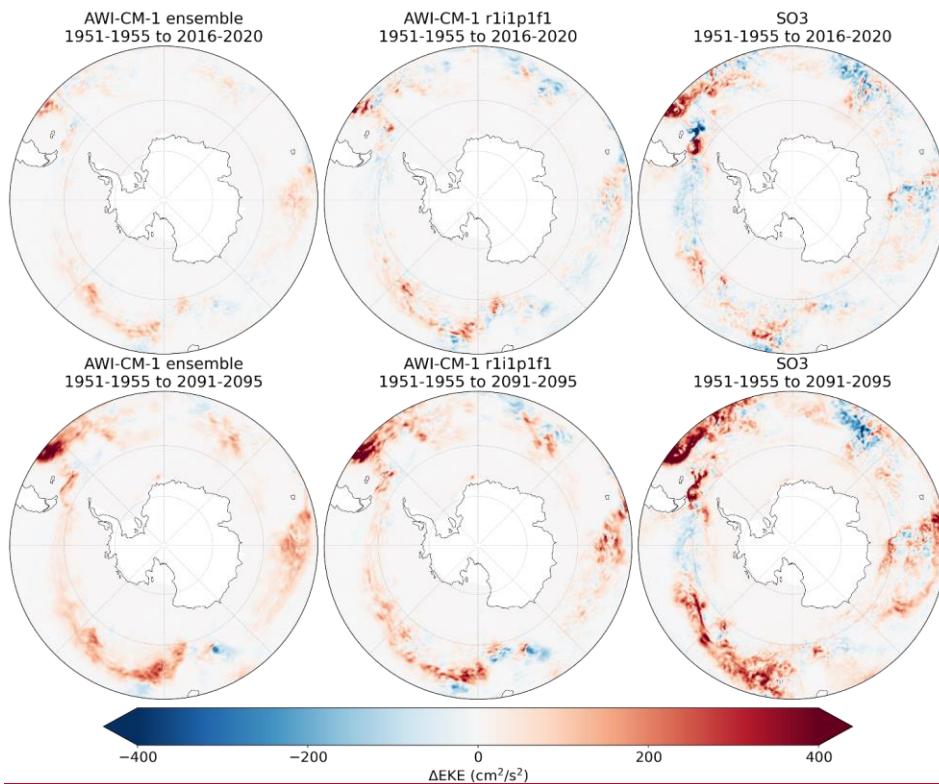
Figure 5. EKE change. Spatial representations of the difference in EKE between **(a-c)** 1951-1955 and

2016-2020, **(d-f)** 1951-1955 and 2091-2095. **a,d)** The AWI-CM-1 ensemble. **b,e)** the first member of the

AWI-CM-1 ensemble. **c,f)** The SO3 simulations.

4 Discussion

    Intensification of eddy activity in the Southern Ocean is now widely accepted as a consequence

of anthropogenic climate change (Hogg et al., 2015; Patara et al., 2016; Martínez-Moreno et al., 2021;

Beech et al., 2022), and is understood to be caused primarily by stronger westerly winds imparting more

energy to the Antarctic Circumpolar Current (Munday et al., 2013; Marshall, 2003). The results presented

468   here reinforce the notion of EKE intensification and further project increased EKE variability as the

469   climate warms (Figure 1, 3). By expressing EKE change in terms of ensemble agreement on a cell-by-cell

470   basis, the results presented here are also able to identify regions of reliable and substantial change as those

471   where flow interacts with major bathymetric features, and high eddy activity is already known to occur

472   (Figure 4). Understanding Analysis of regional changes within the Southern Ocean eddy field hais

473   generally been limited to regions defined by oceanic sectors (Atlantic, Indian, Pacific) (Hogg et al., 2015),

474   or incremental longitudinal delimitations (Patara et al., 2016). By expressing EKE change in terms of

475   ensemble agreement on a cell-by-cell basis, the results presented here are able to identify regions of

476   reliable and substantial change as those where flow interacts with major bathymetric features, and high

477   eddy activity is already known to occur (Figure 4). In future research, regional analyses of both the

478   significance, rate, andor cause of EKE trends could focus on the bathymetrically definedthese regions

479   identified in this analysis to to avoid confounding results with those of physically unrelated change within

480   the chosen geographic delimitationsproduce physically related and consistent results.

481   The consistency of the AWI-CM-1 ensemble in projecting clear EKE rise in the Southern Ocean

482   as a whole suggests that a single ensemble member of five-years simulation length should be sufficient to

483   reliably identify change, even after 1 °C of temperature rise. Despite this, the SO3 simulations fail to

484   reproduce the EKE rise that is already observable through observations (Martínez-Moreno et al., 2021). A

485   potential source for this discrepancy is the uncoupled model setup in the SO3 simulations which omits

486   ocean-atmosphere feedbacks. In this regard, the SO3 simulations experience lower wind stress imparted

487   to the ocean surface than AWI-CM-1 ensemble member one by the same surface winds (Supplementary

488   Figure 4), and a mismatch between peak zonal wind speeds and mean zonal ocean velocities

489   (Supplementary Figure 3). Confounding the comparison further, is the fact that strengthening winds can

490   both increase and dampen eddy activity; as westerlies intensify, the additional energy imparted to the

491   ocean is expected to strengthen eddy activity (Munday et al., 2013; Meredith and Hogg, 2006), but winds

492   are also known to dampen mesoscale activity through eddy killing (Rai et al., 2021) and this impact is

493 greater in uncoupled model configurations (Renault et al., 2016). While the lack of change at 1 °C is
494 difficult to explain, the disagreement is limited to these more subtle changes and the simulations tend to
495 agree on the strong EKE rise at 4 °C of warming.

496 Considering the consistency of the AWI-CM-1 ensemble both in terms of representing regional mean
497 EKE (Supplementary Figure 2), and projecting overall Southern Ocean EKE change (Figure 2), it appears
498 that a larger ensemble of high-resolution simulations is not necessary to assess local mean states and
499 changes over the entire region. This also means that the discrepancies between the SO3 simulations and
500 AWI-CM-1 ensemble remain unexplained. The SO3 simulations failed to reproduce the clear
501 intensification of EKE present in the ensemble at 1 °C of warming(Martínez-Moreno et al., 2021), which
502 has already been identified in observations (Martínez-Moreno et al., 2021). One potential explanation for
503 this is the atmospheric forcing applied to the SO3 simulations which cannot react to oceanic conditions in
504 the same way that the real atmosphere or coupled atmosphere of the AWI-CM-1 ensemble can.
505 Consequently, atmospheric forcing has been found to cause 27% more eddy killing by wind stress than
506 coupled simulations (Renault et al., 2016). Since intensifying wind is widely considered the cause of EKE
507 intensification in the Southern Ocean (Munday et al., 2013; Meredith and Hogg, 2006)(Meredith and
508 Hogg, 2006; Munday et al., 2013; Hogg et al., 2015; Beech et al., 2022), the increase may be counteracted
509 by a simultaneous increase in eddy killing.

510   The remaining discrepancies between eddy activity in SO3 and observations are relatively small,
511 but Assuming that the medium-resolution spin-up simulation effectively imparts a generally equilibrated
512 ocean to the SO3 simulations in terms of baroclinic and barotropic instability, exploring potential sources
513 of disagreement may help to interpret the simulations and guide future modeling endeavorsthe remaining
514 discrepancies between eddy activity in SO3 and observations should be largely identifiable. Greater skew
515 in the distribution of EKE in the modeled dataset (Supplementary Table 2) could reflect multiple modes
516 of circulation or seasonality. While seasonality of eddy activity in the ACC is low, seasonal ice cover
517 likely affects eddy activity in the modeled dataset, and certainly affects the observational dataset by

518   producing gaps in its spatio-temporal coverage. Beyond differences in skew, this could contribute to the

519   greater range of EKE seen in the SO3 simulations by systemically obscuring seasonal conditions from the

520   observational dataset. Regional deficiencies of EKE in SO3 could be explained in terms of grid resolution

521   outside of the study region; resolving the first Rossby radius of deformation with at least two grid points

522   is not enough to comprehensively reproduce mesoscale activity (Hallberg, 2013; Sein et al., 2017), and

523   meaning grid refinement may need to be expanded to upstream regions that impact eddy dynamics in the

524   Southern Ocean. Other sources of bias may include ocean-atmosphere interactions which are absent or

525   unrealistic within the uncoupled simulations (Byrne et al., 2016; Rai et al., 2021; Renault et al., 2016). As

526   well, some small-scale, slow-to-equilibrate ocean processes may be resolved in the high-resolution

527   simulations, but not be integrated long enough for their effects to impact eddy activity (van Westen and

528   Dijkstra, 2021; Rackow et al., 2022). Finally, the gridded altimetry product itself may be responsible for

529   some disagreement, as the along-track data is known to underrepresent eddy activity at scales less than

530   150km and 10 days (Chassignet and Xu, 2017), which will be particularly impactful at high latitudes.

531   To distinguish a meaningful signal of anthropogenic impacts from natural variability, this

532   analysis relies primarily on consistency among ensemble members (Figures 3, 4). This is distinct from

533   more traditional methods like assessment of error relative to observations or ensemble mean, commonly

534   applied to weather forecasting (Ferro et al., 2012), but can be compared to measures of ensemble

535   agreement used extensively in the IPCC reports ADDIN ZOTERO_ITEM CSL_CITATION

536   {"citationID":"UjI4jUc8","properties":{"formattedCitation":"(Frenger et al.,

537   2015)","plainCitation":"(Frenger et al.,

538   2015)","noteIndex":0},"citationItems":[{"id":500,"uris":["http://zotero.org/users/6300652/items/9EPNRS

539   D9"],"itemData":{"id":500,"type":"article-journal","abstract":"Mesoscale eddies are ubiquitous features

540   in the Southern Ocean, yet their phenomenology is not well quantified. To tackle this task, we use satellite

541   observations of sea level anomalies and sea surface temperature (SST) as well as in situ temperature and

542   salinity measurements from profiling floats. Over the period 1997–2010, we identified over a million

543 ~~mesoscale eddy instances and were able to track about 105 of them over 1 month or more. The Antarctic~~
544 ~~Circumpolar Current (ACC), the boundary current systems, and the regions where they interact are hot~~
545 ~~spots of eddy presence, representing also the birth places and graveyards of most eddies. These hot spots~~
546 ~~contrast strongly to areas shallower than about 2000 m, where mesoscale eddies are essentially absent,~~
547 ~~likely due to topographical steering. Anticyclones tend to dominate the southern subtropical gyres, and~~
548 ~~cyclones the northern flank of the ACC. Major causes of regional polarity dominance are larger formation~~
549 ~~numbers and lifespans, with a contribution of differential propagation pathways of long-lived eddies.~~
550 ~~Areas of dominance of one polarity are generally congruent with the same polarity being longer-lived,~~
551 ~~bigger, of larger amplitude, and more intense. Eddies extend down to at least 2000 m. In the ACC, eddies~~
552 ~~show near surface temperature and salinity maxima, whereas eddies in the subtropical areas generally~~
553 ~~have deeper anomaly maxima, presumably inherited from their origin in the boundary currents. The~~
554 ~~temperature and salinity signatures of the average eddy suggest that their tracer anomalies are a result of~~
555 ~~both trapping in the eddy core and stirring.","container-title":"Journal of Geophysical Research:~~
556 ~~Oceans","DOI":"10.1002/2015JC011047","ISSN":"2169-~~
557 ~~9291","issue":"11","language":"en","note":"_eprint:~~
558 ~~https://onlinelibrary.wiley.com/doi/pdf/10.1002/2015JC011047","page":"7413-7449","source":"Wiley~~
559 ~~Online Library","title":"Southern Ocean eddy~~
560 ~~phenomenology","URL":"https://onlinelibrary.wiley.com/doi/abs/10.1002/2015JC011047","volume":"12~~
561 ~~0","author":[{"family":"Frenger","given":"I."},{"family":"Münnich","given":"M."},{"family":"Gruber","~~
562 ~~given":"N."},{"family":"Knutti","given":"R."}],"accessed":{"date-parts":[["2023",5,2]]},"issued":{"date-~~
563 ~~parts":[["2015"]]}}]],"schema":"https://github.com/citation-style-language/schema/raw/master/csl-~~
564 ~~citation.json"} (Frenger et al., 2015)~~ (Fox-Kemper et al., 2021). Performance evaluation relative to
565 observations would undoubtedly point to the high-resolution simulation as superior due to the drastic
566 underrepresentation of EKE in the eddy-permitting ensemble (Figure 1). Yet, the effects of climate
567 change are still apparent in the AWI-CM-1 ensemble (Figure 1, 5), and the AWI-CM-1 dataset has been
568 used to make similar projections of EKE already (Beech et al., 2022). Moreover, the eddy response to

569   forcing seems to be consistent between the model resolutions when expressed in relative (Figure 1g, h, i),

570   rather than absolute terms (Figure 1a, b, c). While more verification of this result is necessary both

571   regionally, and with other models, these results suggest that eddy-permitting resolutions can be

572   interpreted with their shortcomings in mind in order to discern the real-world implications: as is often

573   necessary with model data. Thus, based on the test case of the Southern Ocean, the usefulness of the

574   AWI-CM-1 ensemble and the effectiveness of model simulations in identifying physically significant and

575   reproduceable impacts of climate change may be greater than would be identified using traditional

576   methods and comes at a much lower cost relative to the eddy-resolving simulations.

577   This study has focused on EKE as an evaluation metric for the simulations since mesoscale

578   activity is the primary motivation for increasing ocean model resolution. It has stopped short of assessing

579   the improvements that resolving the mesoscale has on climate and ocean dynamics, many of which are

580   discussed in detail elsewhere (eg. (Hewitt et al., 2017). Rather than repeat an assessment of the benefits of

581   resolving smaller scales, we assume that the accurate reproduction and evolution of eddy activity

582   indicates that these improvements are transferred to broader processes. Certainly, inaccurate simulation of

583   the mesoscale would raise questions regarding the improvements that this mesoscale activity should have

584   on the simulations as a whole. Nonetheless, further evaluation of the modeling approaches employed in

585   this study will be necessary to determine if these methods are appropriate for studying broader elements

586   of the climate system. Since the high-resolution simulations derive their deep-ocean climate primarily

587   from the medium-resolution spin-up simulation, improving the initialization process (Thiria et al., 2023)

588   may be the critical barrier to extending these results from the mixed layer to the deeper ocean.

589   **5 Conclusion**

590   Resolving the ocean mesoscale has become a focus for the climate and ocean modeling

591   community as computational capabilities expand and models become increasingly complex. The benefits

592   that explicitly resolved eddy activity can have on climate simulations are clear (Hewitt et al., 2017; Sein

593   et al., 2017) along with the impact that mesoscale variability has on local (Lachkar et al., 2009; Wang et

594   al., 2017) and global environments (Falkowski et al., 1991; Sallée et al., 2012). However, state-of-the-art

595   climate models will be unable to fully resolve the mesoscale for the foreseeable future, particularly in

596   large-scale modeling endeavors such as CMIP (Hewitt et al., 2020). Thus, modelers must make informed

597   choices regarding the explicit processes needed to answer research questions and where resources must be

598   allocated to achieve specific goals. Existing analysis of resource allocation has typically addressed short-

599   term weather forecasting or the ability to reproduce observations with low error (Ferro et al., 2012), but

600   the question of how to best allocate resources for climate change impact assessment remains. This study

601   has applied several cost-efficient modeling approaches to an analysis of the impacts of climate change on

602   a key focus of high-resolution modeling: the mesoscale. Applying these results to broader climate change

603   impact studies should improve the efficiency of resource allocation and focus modeling studies.

604   Resolution can be dynamically adjusted both spatially, by focusing resources in study regions and where

605   they are necessary to resolve local dynamics, and temporally, by allowing lower-resolution workhorse

606   configurations to perform spin-up and transient runs. Limited simulation length and ensemble size can be

607   sufficient for certain research questions and validation, but simulations must ultimately be designed to

608   meet their specific goals. Where resources are limited, studies may best include a combination of eddy-

609   resolving simulations able to fully capture the local eddy field, as well as eddy-permitting~~present~~

610   simulations that can attest to the significance of results through consistency and repetition.

611   This work represents a contribution to the growing wealth of research that points to an

612   intensification of eddy activity in the Southern Ocean (Hogg et al., 2015; Martínez-Moreno et al., 2021;

613   Beech et al., 2022). The further conclusions that EKE variability may increase and that EKE

614   intensification appears concentrated in key regions based on topography can both expand the present state

615   of knowledge, as well as direct future research. The cost-efficient modelling approaches of regional grid

616   refinement, reduced-resolution spin-up and transient runs, and limited simulation lengths distinguished by

617   longer periods of change are demonstrated to be effective at reproducing change within a more traditional

618   eddy-permitting ensemble. When resources are limited and resolution demands are high, these approaches

619 can be adapted to address specific research questions. Where assessing the robustness of change is

620 critical, the complimentary eddy-permitting ensemble represents an effective, low-cost supplement to the

621 high-resolution simulations.

622

623

624

Data Availability

Geostrophic velocities derived from satellite altimetry data are publicly available at https://doi.org/10.48670/moi-00148. Daily sea surface height data from AWI-CM-1-1-MR in CMIP6 used to compute geostrophic velocities in this study is archived at the World Data Center for Climate at the DKRZ (https://doi.org/10.26050/WDCC/C6sCMAWAWM, https://doi.org/10.26050/WDCC/C6sSPAWAWM) (Semmler et al., 2022a, b). Model output from AWI-CM-1-1-MR in the CMIP6 framework, including all variables used to force the standalone ocean simulations conducted for this study, is publicly available at https://doi.org/10.22033/ESGF/CMIP6.359 (Semmler et al., 2018). Eddy kinetic energy datasets calculated from FESOM output velocities are available at https://doi.org/10.5281/zenodo.8046792(https://doi.org/10.5281/zenodo.8046792) (Beech, 2023b).

Code Availability

Source code for the ocean model FESOM2 is available at (https:/doi.org/ 10.5281/zenodo.7737061) (patrickscholz et al., 2023). Code used for data analysis and visualization in this study is publicly available at (https://doi.org/10.5281/zenodo.10025361https://doi.org/10.5281/zenodo.8046783) (Beech, 2023a). Code used to calculate geostrophic velocities from sea surface height data from AWI-CM-1-1-MR is available from https://doi.org/10.5281/zenodo.7050573.

Author Contributions

NB, TJ, TR, and TS conceived of the study. NB carried out the simulations, analyzed the data, and drafted the manuscript. All authors reviewed the manuscript.

Competing Interests

The authors declare no competing interests.

648   **Acknowledgements**

649   The work described in this paper has received funding from the Helmholtz Association through

650   the project 'Advanced Earth System Model Capacity' (project leader: T.J., support code: ZT-0003) in the

651   frame of the initiative 'Zukunftsthemen'. The content of the paper is the sole responsibility of the authors

652   and it does not represent the opinion of the Helmholtz Association, and the Helmholtz Association is not

653   responsible for any use that might be made of information contained. TJ acknowledges the EERIE project

654   funded under the EU Horizon Europe programme (grant number 101081383). TR acknowledges support

655   from the European Commission's Horizon 2020 collaborative project NextGEMS (grant number

656   101003470). This work used resources of the Deutsches Klimarechenzentrum (DKRZ) granted by its

657   Scientific Steering Committee (WLA) under project ID 995. The CMIP data used in this study were

658   replicated and made available by the DKRZ.

659

660

References

Auger, M., Prandi, P., and Sallée, J.-B.: Southern ocean sea level anomaly in the sea ice-covered sector from multimission satellite observations, Sci. Data, 9, 70, https://doi.org/10.1038/s41597-022-01166-z, 2022.

Auger, M., Sallée, J.-B., Thompson, A. F., Pauthenet, E., and Prandi, P.: Southern Ocean Ice-Covered Eddy Properties From Satellite Altimetry, J. Geophys. Res. Oceans, 128, e2022JC019363, https://doi.org/10.1029/2022JC019363, 2023.

Ballarotta, M., Ubelmann, C., Pujol, M.-I., Taburet, G., Fournier, F., Legeais, J.-F., Faugère, Y., Delepoulle, A., Chelton, D., Dibarboure, G., and Picot, N.: On the resolutions of ocean altimetry maps, Ocean Sci., 15, 1091–1109, https://doi.org/10.5194/os-15-1091-2019, 2019.

Beech, N.: Beech_et_al_cost_efficient_SO: Revision, https://doi.org/10.5281/zenodo.10025361, 2023a.

Beech, N.: Processed EKE from FESOM-SO3 (1.0), https://doi.org/10.5281/zenodo.8046792, 2023b.

Beech, N., Rackow, T., Semmler, T., Danilov, S., Wang, Q., and Jung, T.: Long-term evolution of ocean eddy activity in a warming world, Nat. Clim. Change, 12, 910–917, https://doi.org/10.1038/s41558-022-01478-3, 2022.

Bishop, S. P., Gent, P. R., Bryan, F. O., Thompson, A. F., Long, M. C., and Abernathey, R.: Southern Ocean Overturning Compensation in an Eddy-Resolving Climate Simulation, J. Phys. Oceanogr., 46, 1575–1592, https://doi.org/10.1175/JPO-D-15-0177.1, 2016.

Bronselaer, B., Winton, M., Griffies, S. M., Hurlin, W. J., Rodgers, K. B., Sergienko, O. V., Stouffer, R. J., and Russell, J. L.: Change in future climate due to Antarctic meltwater, Nature, 564, 53–58, https://doi.org/10.1038/s41586-018-0712-z, 2018.

Byrne, D., Münnich, M., Frenger, I., and Gruber, N.: Mesoscale atmosphere ocean coupling enhances the transfer of wind energy into the ocean, Nat. Commun., 7, ncomms11867, https://doi.org/10.1038/ncomms11867, 2016.

Chassignet, E. P. and Xu, X.: Impact of Horizontal Resolution (1/12° to 1/50°) on Gulf Stream Separation, Penetration, and Variability, J. Phys. Oceanogr., 47, 1999–2021, https://doi.org/10.1175/JPO-D-17-0031.1, 2017.

D'Agostino, R. B. and Belanger, A.: A Suggestion for Using Powerful and Informative Tests of Normality, Am. Stat., 44, 316–321, https://doi.org/10.2307/2684359, 1990.

Danilov, S.: Ocean modeling on unstructured meshes, Ocean Model., 69, 195–210, https://doi.org/10.1016/j.ocemod.2013.05.005, 2013.

Danilov, S.: On the Resolution of Triangular Meshes, J. Adv. Model. Earth Syst., 14, e2022MS003177, https://doi.org/10.1029/2022MS003177, 2022.

Danilov, S., Sidorenko, D., Wang, Q., and Jung, T.: The Finite-volumE Sea ice–Ocean Model (FESOM2), Geosci. Model Dev., 10, 765–789, https://doi.org/10.5194/gmd-10-765-2017, 2017.

696 Durbin, J. and Watson, G. S.: Testing for Serial Correlation in Least Squares Regression. I, Biometrika, 37,
697 409–428, https://doi.org/10.1093/biomet/37.3-4.409, 1950.

698 Eyring, V., Bony, S., Meehl, G. A., Senior, C. A., Stevens, B., Stouffer, R. J., and Taylor, K. E.: Overview of
699 the Coupled Model Intercomparison Project Phase 6 (CMIP6) experimental design and organization,
700 Geosci. Model Dev., 9, 1937–1958, https://doi.org/10.5194/gmd-9-1937-2016, 2016.

701 Falkowski, P. G., Ziemann, D., Kolber, Z., and Bienfang, P. K.: Role of eddy pumping in enhancing primary
702 production in the ocean, Nature, 352, 55–58, https://doi.org/10.1038/352055a0, 1991.

703 Ferrari, R., Griffies, S. M., Nurser, A. J. G., and Vallis, G. K.: A boundary-value problem for the
704 parameterized mesoscale eddy transport, Ocean Model., 32, 143–156,
705 https://doi.org/10.1016/j.ocemod.2010.01.004, 2010.

706 Ferro, C. A. T., Jupp, T. E., Lambert, F. H., Huntingford, C., and Cox, P. M.: Model complexity versus
707 ensemble size: allocating resources for climate prediction, Philos. Trans. R. Soc. Math. Phys. Eng. Sci.,
708 370, 1087–1099, https://doi.org/10.1098/rsta.2011.0307, 2012.

709 Fisher, R. A.: The moments of the distribution for normal samples of measures of departure from
710 normality, Proc. R. Soc. Lond. Ser. Contain. Pap. Math. Phys. Character, 130, 16–28,
711 https://doi.org/10.1098/rspa.1930.0185, 1997.

712 Frölicher, T. L., Sarmiento, J. L., Paynter, D. J., Dunne, J. P., Krasting, J. P., and Winton, M.: Dominance of
713 the Southern Ocean in Anthropogenic Carbon and Heat Uptake in CMIP5 Models, J. Clim., 28, 862–886,
714 https://doi.org/10.1175/JCLI-D-14-00117.1, 2015.

715 Gent, P. R. and McWilliams, J. C.: Isopycnal Mixing in Ocean Circulation Models, J. Phys. Oceanogr., 20,
716 150–155, https://doi.org/10.1175/1520-0485(1990)020<0150:IMIOCM>2.0.CO;2, 1990.

717 Haarsma, R. J., Roberts, M. J., Vidale, P. L., Senior, C. A., Bellucci, A., Bao, Q., Chang, P., Corti, S., Fučkar,
718 N. S., Guemas, V., von Hardenberg, J., Hazeleger, W., Kodama, C., Koenigk, T., Leung, L. R., Lu, J., Luo, J.-
719 J., Mao, J., Mizielinski, M. S., Mizuta, R., Nobre, P., Satoh, M., Scoccimarro, E., Semmler, T., Small, J., and
720 von Storch, J.-S.: High Resolution Model Intercomparison Project (HighResMIP v1.0) for CMIP6, Geosci.
721 Model Dev., 9, 4185–4208, https://doi.org/10.5194/gmd-9-4185-2016, 2016.

722 Hallberg, R.: Using a resolution function to regulate parameterizations of oceanic mesoscale eddy
723 effects, Ocean Model., 72, 92–103, https://doi.org/10.1016/j.ocemod.2013.08.007, 2013.

724 Hewitt, H. T., Bell, M. J., Chassignet, E. P., Czaja, A., Ferreira, D., Griffies, S. M., Hyder, P., McClean, J. L.,
725 New, A. L., and Roberts, M. J.: Will high-resolution global ocean models benefit coupled predictions on
726 short-range to climate timescales?, Ocean Model., 120, 120–136,
727 https://doi.org/10.1016/j.ocemod.2017.11.002, 2017.

728 Hewitt, H. T., Roberts, M., Mathiot, P., Biastoch, A., Blockley, E., Chassignet, E. P., Fox-Kemper, B., Hyder,
729 P., Marshall, D. P., Popova, E., Treguier, A.-M., Zanna, L., Yool, A., Yu, Y., Beadling, R., Bell, M., Kuhlbrodt,
730 T., Arsouze, T., Bellucci, A., Castruccio, F., Gan, B., Putrasahan, D., Roberts, C. D., Van Roekel, L., and
731 Zhang, Q.: Resolving and Parameterising the Ocean Mesoscale in Earth System Models, Curr. Clim.
732 Change Rep., 6, 137–152, https://doi.org/10.1007/s40641-020-00164-w, 2020.

Hogg, A. McC., Meredith, M. P., Chambers, D. P., Abrahamsen, E. P., Hughes, C. W., and Morrison, A. K.: Recent trends in the Southern Ocean eddy field, J. Geophys. Res. Oceans, 120, 257–267, https://doi.org/10.1002/2014JC010470, 2015.

Irving, D., Hobbs, W., Church, J., and Zika, J.: A Mass and Energy Conservation Analysis of Drift in the CMIP6 Ensemble, J. Clim., 34, 3157–3170, https://doi.org/10.1175/JCLI-D-20-0281.1, 2021.

Jungclaus, J. H., Lorenz, S. J., Schmidt, H., Brovkin, V., Brüggemann, N., Chegini, F., Crüger, T., De-Vrese, P., Gayler, V., Giorgetta, M. A., Gutjahr, O., Haak, H., Hagemann, S., Hanke, M., Ilyina, T., Korn, P., Kröger, J., Linardakis, L., Mehlmann, C., Mikolajewicz, U., Müller, W. A., Nabel, J. E. M. S., Notz, D., Pohlmann, H., Putrasahan, D. A., Raddatz, T., Ramme, L., Redler, R., Reick, C. H., Riddick, T., Sam, T., Schneck, R., Schnur, R., Schupfner, M., von Storch, J.-S., Wachsmann, F., Wieners, K.-H., Ziemen, F., Stevens, B., Marotzke, J., and Claussen, M.: The ICON Earth System Model Version 1.0, J. Adv. Model. Earth Syst., 14, e2021MS002813, https://doi.org/10.1029/2021MS002813, 2022.

Lachkar, Z., Orr, J. C., Dutay, J. C., and Delecluse, P.: On the role of mesoscale eddies in the ventilation of Antarctic intermediate water, Deep-Sea Res. Part Oceanogr. Res. Pap., 56, 909–925, https://doi.org/10.1016/j.dsr.2009.01.013, 2009.

Landschützer, P., Gruber, N., Haumann, F. A., Rödenbeck, C., Bakker, D. C. E., van Heuven, S., Hoppema, M., Metzl, N., Sweeney, C., Takahashi, T., Tilbrook, B., and Wanninkhof, R.: The reinvigoration of the Southern Ocean carbon sink, Science, 349, 1221–1224, https://doi.org/10.1126/science.aab2620, 2015.

Large, W. G., McWilliams, J. C., and Doney, S. C.: Oceanic vertical mixing: A review and a model with a nonlocal boundary layer parameterization, Rev. Geophys., 32, 363–403, https://doi.org/10.1029/94RG01872, 1994.

Marshall, G. J.: Trends in the Southern Annular Mode from Observations and Reanalyses, J. Clim., 16, 4134–4143, https://doi.org/10.1175/1520-0442(2003)016<4134:TITSAM>2.0.CO;2, 2003.

Marshall, J., Jones, H., Karsten, R., and Wardle, R.: Can Eddies Set Ocean Stratification?, J. Phys. Oceanogr., 32, 26–38, https://doi.org/10.1175/1520-0485(2002)032<0026:CESOS>2.0.CO;2, 2002.

Martínez-Moreno, J., Hogg, A. McC., England, M. H., Constantinou, N. C., Kiss, A. E., and Morrison, A. K.: Global changes in oceanic mesoscale currents over the satellite altimetry record, Nat. Clim. Change, 11, 397–403, https://doi.org/10.1038/s41558-021-01006-9, 2021.

Marzocchi, A., Hirschi, J. J.-M., Holliday, N. P., Cunningham, S. A., Blaker, A. T., and Coward, A. C.: The North Atlantic subpolar circulation in an eddy-resolving global ocean model, J. Mar. Syst., 142, 126–143, https://doi.org/10.1016/j.jmarsys.2014.10.007, 2015.

Meredith, M. P. and Hogg, A. M.: Circumpolar response of Southern Ocean eddy activity to a change in the Southern Annular Mode, Geophys. Res. Lett., 33, https://doi.org/10.1029/2006GL026499, 2006.

Munday, D. R., Johnson, H. L., and Marshall, D. P.: Eddy Saturation of Equilibrated Circumpolar Currents, J. Phys. Oceanogr., 43, 507–532, https://doi.org/10.1175/JPO-D-12-095.1, 2013.

O'Neill, B. C., Tebaldi, C., van Vuuren, D. P., Eyring, V., Friedlingstein, P., Hurtt, G., Knutti, R., Kriegler, E., Lamarque, J.-F., Lowe, J., Meehl, G. A., Moss, R., Riahi, K., and Sanderson, B. M.: The Scenario Model

770   Intercomparison Project (ScenarioMIP) for CMIP6, Geosci. Model Dev., 9, 3461–3482,
771   https://doi.org/10.5194/gmd-9-3461-2016, 2016.

772   O'Neill, B. C., Kriegler, E., Ebi, K. L., Kemp-Benedict, E., Riahi, K., Rothman, D. S., van Ruijven, B. J., van
773   Vuuren, D. P., Birkmann, J., Kok, K., Levy, M., and Solecki, W.: The roads ahead: Narratives for shared
774   socioeconomic pathways describing world futures in the 21st century, Glob. Environ. Change, 42, 169–
775   180, https://doi.org/10.1016/j.gloenvcha.2015.01.004, 2017.

776   Patara, L., Böning, C. W., and Biastoch, A.: Variability and trends in Southern Ocean eddy activity in 1/12°
777   ocean model simulations, Geophys. Res. Lett., 43, 4517–4523, https://doi.org/10.1002/2016GL069026,
778   2016.

779   patrickscholz, dsidoren, Koldunov, N., Hegewald, J., rakowsk, Streffing, J., Rackow, T., ogurses,
780   helgegoessling, Guibert, D., qiangclimate, cwekerle, Oord, G. van den, jrberlin, Miguel, Gierz, P., and
781   Cheedela, S. K.: FESOM/fesom2: FESOM2.5, , https://doi.org/10.5281/zenodo.7737061, 2023.

782   Pauling, A. G., Smith, I. J., Langhorne, P. J., and Bitz, C. M.: Time-Dependent Freshwater Input From Ice
783   Shelves: Impacts on Antarctic Sea Ice and the Southern Ocean in an Earth System Model, Geophys. Res.
784   Lett., 44, 10,454-10,461, https://doi.org/10.1002/2017GL075017, 2017.

785   Price, J. F., Weller, R. A., and Schudlich, R. R.: Wind-Driven Ocean Currents and Ekman Transport,
786   Science, 238, 1534–1538, https://doi.org/10.1126/science.238.4833.1534, 1987.

787   Rackow, T., Danilov, S., Goessling, H. F., Hellmer, H. H., Sein, D. V., Semmler, T., Sidorenko, D., and Jung,
788   T.: Delayed Antarctic sea-ice decline in high-resolution climate change simulations, Nat. Commun., 13,
789   637, https://doi.org/10.1038/s41467-022-28259-y, 2022.

790   Rai, S., Hecht, M., Maltrud, M., and Aluie, H.: Scale of oceanic eddy killing by wind from global satellite
791   observations, Sci. Adv., 7, eabf4920, https://doi.org/10.1126/sciadv.abf4920, 2021.

792   Renault, L., Molemaker, M. J., McWilliams, J. C., Shchepetkin, A. F., Lemarié, F., Chelton, D., Illig, S., and
793   Hall, A.: Modulation of Wind Work by Oceanic Current Interaction with the Atmosphere, J. Phys.
794   Oceanogr., 46, 1685–1704, https://doi.org/10.1175/JPO-D-15-0232.1, 2016.

795   Ringler, T., Petersen, M., Higdon, R. L., Jacobsen, D., Jones, P. W., and Maltrud, M.: A multi-resolution
796   approach to global ocean modeling, Ocean Model., 69, 211–232,
797   https://doi.org/10.1016/j.ocemod.2013.04.010, 2013.

798   Sallée, J.-B., Matear, R. J., Rintoul, S. R., and Lenton, A.: Localized subduction of anthropogenic carbon
799   dioxide in the Southern Hemisphere oceans, Nat. Geosci., 5, 579–584,
800   https://doi.org/10.1038/ngeo1523, 2012.

801   Scholz, P., Sidorenko, D., Gurses, O., Danilov, S., Koldunov, N., Wang, Q., Sein, D., Smolentseva, M.,
802   Rakowsky, N., and Jung, T.: Assessment of the Finite-volumE Sea ice-Ocean Model (FESOM2.0) – Part 1:
803   Description of selected key model elements and comparison to its predecessor version, Geosci. Model
804   Dev., 12, 4875–4899, https://doi.org/10.5194/gmd-12-4875-2019, 2019.

805   Scholz, P., Sidorenko, D., Danilov, S., Wang, Q., Koldunov, N., Sein, D., and Jung, T.: Assessment of the
806   Finite VolumE Sea Ice Ocean Model (FESOM2.0), Part II: Partial bottom cells, embedded sea ice and

807   vertical mixing library CVMIX, Climate and Earth system modeling, https://doi.org/10.5194/gmd-2021-
808   94, 2021.

809   Sein, D. V., Koldunov, N. V., Danilov, S., Wang, Q., Sidorenko, D., Fast, I., Rackow, T., Cabos, W., and Jung,
810   T.: Ocean Modeling on a Mesh With Resolution Following the Local Rossby Radius, J. Adv. Model. Earth
811   Syst., 9, 2601–2614, https://doi.org/10.1002/2017MS001099, 2017.

812   Semmler, T., Danilov, S., Rackow, T., Sidorenko, D., Barbi, D., Hegewald, J., Sein, D., Wang, Q., and Jung,
813   T.: AWI AWI-CM1.1MR model output prepared for CMIP6 CMIP,
814   https://doi.org/10.22033/ESGF/CMIP6.359, 2018.

815   Semmler, T., Danilov, S., Gierz, P., Goessling, H. F., Hegewald, J., Hinrichs, C., Koldunov, N., Khosravi, N.,
816   Mu, L., Rackow, T., Sein, D. V., Sidorenko, D., Wang, Q., and Jung, T.: Simulations for CMIP6 With the
817   AWI Climate Model AWI-CM-1-1, J. Adv. Model. Earth Syst., 12, e2019MS002009,
818   https://doi.org/10.1029/2019MS002009, 2020.

819   Semmler, T., Danilov, S., Rackow, T., Sidorenko, D., Barbi, D., Hegewald, J., Sein, D., Wang, Q., and Jung,
820   T.: CMIP6_supplemental CMIP AWI AWI-CM-1-1-MR, https://doi.org/10.26050/WDCC/C6sCMAWAWM,
821   2022a.

822   Semmler, T., Danilov, S., Rackow, T., Sidorenko, D., Barbi, D., Hegewald, J., Sein, D., Wang, Q., and Jung,
823   T.: CMIP6_supplemental ScenarioMIP AWI AWI-CM-1-1-MR,
824   https://doi.org/10.26050/WDCC/C6sSPAWAWM, 2022b.

825   Taburet, G., Sanchez-Roman, A., Ballarotta, M., Pujol, M.-I., Legeais, J.-F., Fournier, F., Faugere, Y., and
826   Dibarboure, G.: DUACS DT2018: 25 years of reprocessed sea level altimetry products, Ocean Sci., 15,
827   1207–1224, https://doi.org/10.5194/os-15-1207-2019, 2019.

828   Thiria, S., Sorror, C., Archambault, T., Charantonis, A., Bereziat, D., Mejia, C., Molines, J.-M., and Crépon,
829   M.: Downscaling of ocean fields by fusion of heterogeneous observations using Deep Learning
830   algorithms, Ocean Model., 182, 102174, https://doi.org/10.1016/j.ocemod.2023.102174, 2023.

831   Wang, Q., Danilov, S., Sidorenko, D., Timmermann, R., Wekerle, C., Wang, X., Jung, T., and Schröter, J.:
832   The Finite Element Sea Ice-Ocean Model (FESOM) v.1.4: formulation of an ocean general circulation
833   model, Geosci. Model Dev., 7, 663–693, https://doi.org/10.5194/gmd-7-663-2014, 2014.

834   Wang, Y., Claus, M., Greatbatch, R. J., and Sheng, J.: Decomposition of the Mean Barotropic Transport in
835   a High-Resolution Model of the North Atlantic Ocean, Geophys. Res. Lett., 44, 11,537-11,546,
836   https://doi.org/10.1002/2017GL074825, 2017.

837   van Westen, R. M. and Dijkstra, H. A.: Ocean eddies strongly affect global mean sea-level projections,
838   Sci. Adv., 7, eabf1674, https://doi.org/10.1126/sciadv.abf1674, 2021.

839   Yu, X., Ponte, A. L., Lahaye, N., Caspar-Cohen, Z., and Menemenlis, D.: Geostrophy Assessment and
840   Momentum Balance of the Global Oceans in a Tide- and Eddy-Resolving Model, J. Geophys. Res. Oceans,
841   126, e2021JC017422, https://doi.org/10.1029/2021JC017422, 2021.

842